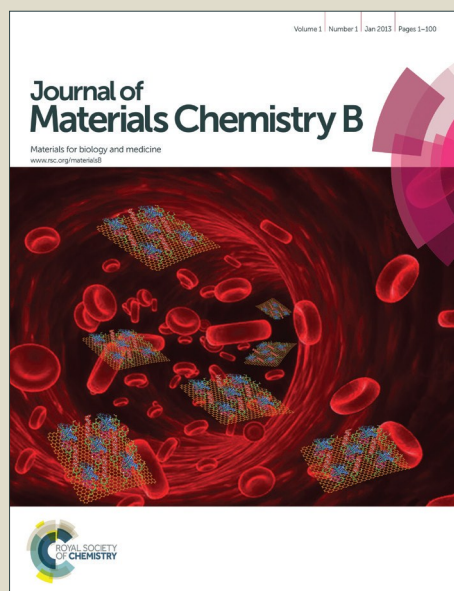


Journal of Materials Chemistry B

Accepted Manuscript



This is an *Accepted Manuscript*, which has been through the Royal Society of Chemistry peer review process and has been accepted for publication.

Accepted Manuscripts are published online shortly after acceptance, before technical editing, formatting and proof reading. Using this free service, authors can make their results available to the community, in citable form, before we publish the edited article. We will replace this *Accepted Manuscript* with the edited and formatted *Advance Article* as soon as it is available.

You can find more information about *Accepted Manuscripts* in the [Information for Authors](#).

Please note that technical editing may introduce minor changes to the text and/or graphics, which may alter content. The journal's standard [Terms & Conditions](#) and the [Ethical guidelines](#) still apply. In no event shall the Royal Society of Chemistry be held responsible for any errors or omissions in this *Accepted Manuscript* or any consequences arising from the use of any information it contains.



Journal Name

ARTICLE

An Electrochemical Bifunctional Sensor for the detection of Nitrite and Hydrogen peroxide Based on Layer-by-Layer Multilayer Films of Cationic Phthalocyanine Cobalt (II) and Carbon Nanotubes†

Received 00th January 20xx,
Accepted 00th January 20xx

DOI: 10.1039/x0xx00000x

www.rsc.org/

Jialin Zhang,^a Zhimin Chen,^{*a} Hao Wu,^a Feng Wu,^a Chunying He,^a Bin Wang,^a Yiqun Wu,^{a, b} and Zhiyu Ren^{*a}

As the vital biological mediators, the accurate detection of nitrite (NO₂⁻) and hydrogen peroxide (H₂O₂) is desirable for clinical monitoring and diagnosis. Herein, cationic 2,9,16,23-tetra[4-(N-methyl) pyridinyloxy] phthalocyanine cobalt(II) ([TMPyPcCo]⁴⁺) and acid-treated multiwalled carbon nanotube (aCNTs) were alternative self-assembled on the glassy carbon electrode (GCE) by means of the electrostatic interaction, leading to a 3D loose and interconnected assembly of [TMPyPcCo/aCNTs]_n multilayer films. In the [TMPyPcCo/aCNTs]_n films, [TMPyPcCo]⁴⁺ is anchored onto the surface of aCNTs without any inert polymer binders, which is beneficial to expose more active sites for electrocatalysis. The effective combination of [TMPyPcCo]⁴⁺ and aCNTs brings many advantages in electrochemical detection, involving fast oriented transmission of charges, permeable channels for ion adsorption and transport, and more sensing sites, thus the [TMPyPcCo/aCNTs]_n films display excellent electrochemical sensitivity towards both NO₂⁻ and H₂O₂. The responses of NO₂⁻ and H₂O₂ vary linearly with respect to the concentration from 5 μM to 30 mM and 10 μM to 9 mM. Furthermore, the superior cycling stability, reproducibility, and selectivity make [TMPyPcCo/aCNTs]_n films suitable for the real samples.

Introduction

Real-time and accurate detection of biological mediator (especially nitrite and hydrogen peroxide) *in vivo* not only can reveal the intrinsic relationships between small molecules and biological processes, but can also be conducive to diseases monitoring and diagnosis.^[1,2] As markers for NO formation in biological fluids,^[3] the level of nitrite (NO₂⁻) is connected with various diseases and physiologic functions, such as cystitis, gastroenteritis, and cardiac or renal allograft rejections.^[4] Furthermore, owing to its highly toxic, dramatic increase of NO₂⁻ levels in biological fluids will cause methemoglobinemia,^[4] esophageal cancer,^[5] and fetal malformation^[6] etc. On the other hand, hydrogen peroxide (H₂O₂) is an important intermediate or product in many enzymatic reactions.^[7] H₂O₂ is cytotoxic to cells and tissues, although it is a signal molecule in the regulation of a wide variety of biological processes. Therefore, development of a reliable, rapid and simple detection method for NO₂⁻ and H₂O₂ is of great significance.^[8]

Several analytical methods have been developed for NO₂⁻ or H₂O₂

determination by far, including chemiluminescence,^[9] fluorescence spectrophotometry,^[10] microchip capillary electrophoresis,^[11] high performance liquid chromatography,^[12] and electrochemical sensors.^[13-15] Accompanied by the rapid development of nanotechnology, the electrochemical sensors based on various electrocatalysts display more advantages compared to others, in terms of high sensitivities, rapid responses, simple operation and real-time analysis, and so on.^[16] In particular, the determining various substrates can be achieved easily by controlling the potentials. Actually, the electrochemical determination of NO₂⁻ and H₂O₂ usually involves a large overpotential and low sensitivity at the surfaces of the unmodified glassy carbon electrode (GCE). Therefore, to improve the electrocatalysis for NO₂⁻ and H₂O₂, the high-efficient electrocatalysts and appropriate electrodes surface modification technology are key issues.^[17-24]

Metallo-phthalocyanines (MPcs) with the planar 18 π-electron conjugated systems, are a well-known class of N4-macrocyclic metal compounds.^[25-27] Due to their high chemical and thermal stability, designed flexibility, varied coordinated metals, diverse substitutional alternatives and interesting electrochemical properties, MPcs are widely used as sensing materials for the detection of biological and environmental compounds, such as O₂, H₂O₂, NO₂⁻, thiols, thiocyanate, dopamine, epinephrine, and so on.^[28,29] However, their intrinsically poor conductivity and low solubility in solvent restrict the detection performance seriously. The former often blocks electron transport, and the latter generally affects the uniformity of sensing devices, resulting in the low detection response, poor repeatability and stability, respectively. To overcome the poor conductivity of MPc, conductive agents were

^a Key Laboratory of Functional Inorganic Material Chemistry (Ministry of Education of China), School of Chemistry and Materials Science, Heilongjiang University, Harbin 150080, People's Republic of China.

^b Shanghai Institutes of Optics and Fine Mechanics, Chinese Academy of Sciences, Shanghai 201800, People's Republic of China.

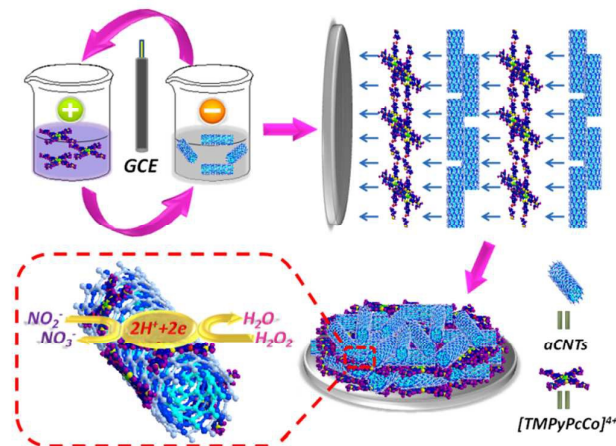
* Corresponding author E-mail: zmchen@siom.ac.cn; zyren@hliu.edu.cn

† Electronic Supplementary Information (ESI) available: Experimental details, additional structural and compositional characterizations, and sensing performance comparison. See DOI: 10.1039/x0xx00000x

often introduced into the detection systems.^[30] Carbon nanotube (CNT) is an attractive option, because CNTs have excellent electrical conductivity and unique one-dimensional structure for the rapidly oriented electronic transmission.^[31-33] Moreover, due to the loose and interlaced structure, the resulting CNT-based sensors offer large accessible surface area and numerous exposed active sites for sensing.^[34,35] Therefore, many studies indicate that the MPC/CNTs hybrids synthesized by π - π interaction display high sensitivity, often surpassing pristine MPCs and CNTs.^[36] However, there is no distinguishing improvement in the case of the repeatability and stability, which is mainly attributed to the unmanageable architecture and characteristics of sensing devices generated by the spontaneous non-covalent bonding between MPCs and CNTs.

In addition, as mentioned above, the electrode modification method is an important factor for sensing performance. Generally, electrochemical tests require the effective immobilization of MPC/CNTs hybrids on GCE surfaces with polymer binders (polytetrafluoroethylene, Nafion, or other polyelectrolytes). In this case the inert polymer binder may block active sites and inhibit charge transportation and matter diffusion, leading to reduced catalytic activity.^[37,38] Meanwhile, the poor mechanical strength and electric conductivity between catalysts and GCEs also limit the practical application. It may easily be conceived that the direct growth of electrocatalysts on GCEs without any binder is an effective strategy in the improvement of mechanical strength, electric conductivity, and exploring of active sites. Layer by layer (LBL) assembly driven by the sequential adsorption of negative and positive charged materials, is straightforward and remarkably low cost for constructing thin films with finely controlled molecular architecture and composition.^[39-41] The thickness of Lbl film can be precisely controlled through adjusting the layer-pair number.^[42] Although it is a facile technique to fabricate versatile films,^[43] there are apparently very few studies about MPC/CNTs sensors, directly LBL assembling of ionic MPCs and CNTs with opposite charge on the surface of GCE.

Based on these considerations, here, a novel electrochemical bifunctional sensor was constructed by LBL electrostatic interaction assembly using cationic 2,9,16,23-tetra[4-(N-methyl)pyridinyloxy]phthalocyanine cobalt(II) sulfate ([TMPyPcCo]⁴⁺) as positive charge and acid-treated multiwalled carbon nanotube (aCNTs) as negative charge (as shown in Scheme 1). As the NO₂⁻ and H₂O₂ sensors, the resulting [TMPyPcCo/aCNTs]_n multilayer films without any polymer binders exhibits high sensitivity, selectivity, repeatability and stability.



Scheme 1. A schematic illustration of the LBL assembly of [TMPyPcCo/aCNTs]_n multilayer films on GCE.

Experimental

2.1 Reagents

2,9,16,23-Tetra[4-(N-methyl)pyridinyloxy]phthalocyanine cobalt(II) sulfate ([TMPyPcCo](SO₄)₂) was synthesized by template-reaction method in the presence of 1,8-diazabicyclo[5,4,0]undec-7-ene (DBU) (see ESI[†] for experimental details). 4-nitrophthalonitrile (99% purity) and DBU (98% purity) were purchased from Sigma-Aldrich Co. LLC. 4-Hydroxypyridine (97% purity) was purchased from Aladdin Shanghai Biochemical Technology Co. Ltd. (Shanghai, China). Multiwalled carbon nanotube (MWCNTs, >95%) was purchased from Shenzhen Nanotech Port Co. Ltd. (Shenzhen, China). Acidified MWCNT (aCNT) was prepared by a mature method.^[36] Deionized water (DI water, 18.2 ΩM) was prepared with a Milli-Q system (Millipore Corp. Bedford, MA, USA). Various pH values of phosphate buffer solutions (PBS, 0.1 M) were prepared by mixing standard stock solutions of NaH₂PO₄ and Na₂HPO₄. All other reagents are analytical grade and were used as received from the suppliers without further purification.

2.2 Preparation of [TMPyPcCo/aCNTs]_n multilayer films

The [TMPyPcCo/aCNTs]_n multilayer films were self-assembled on the pretreated substrates, glassy carbon electrode (GCE) and indium tin oxide (ITO) glass (see ESI[†] for pretreatment details), using the electrostatic layer-by-layer (LBL) deposition technique. In a typical procedure, the pretreated substrate was firstly immersed into an aqueous solution of [TMPyPcCo]⁴⁺ (2 mg/mL) for 10 min and washed thoroughly with DI water. After blow-dried with N₂, it was dipped into a suspension of aCNTs (1 mg/mL) for 10 min and also washed with DI water and blow-dried with N₂. Following similar procedure, the adsorption steps of [TMPyPcCo]⁴⁺ and aCNTs could be repeated as many times as desired to prepare the LBL assembled [TMPyPcCo/aCNTs]_n multilayer films (*n* is the number of bilayer including a layer of [TMPyPcCo]⁴⁺ and a layer of aCNTs).^[44] For comparison, the [TMPyPcCo](SO₄)₂/GCE and aCNTs/GCE were also fabricated by the similar procedures. In these case, the GCE was

only immersed into the $[\text{TMPyPcCo}]^{4+}$ solution or aCNTs solution for 10 min, which is repeated as twelve times.

2.3 Characterization

The UV-Vis absorption spectra of $[\text{TMPyPcCo}]^{4+}$ and aCNT solutions and the $[\text{TMPyPcCo/aCNTs}]_n$ multilayer films on ITO substrates were measured with a Lambda 35 UV-vis spectrometer (Perkin-Elmer, USA). The Raman spectra were executed with a HR800 Raman spectrophotometer (HORIBA Jobin Yvon Company) excited by a laser with 457.9 nm wavelength. FT-IR spectra were recorded on a Nicolet FT-IR NEXUS spectrometer (Thermo Scientific). Scanning electron microscopy (SEM) images were determined by a Hitachi S-4800 field emission scanning electron microscope operating at 15 kV. Transmission electron microscopy (TEM) was performed on a JEM-3010 electron microscope (JEOL, Japan) with an acceleration voltage of 300 kV. X-ray photoelectron spectroscopy (XPS) measures were performed with an AXIS ULTRA DLD. All electrochemical measurements were performed on a computer-controlled CHI760D electrochemical workstation (CH Instrument, China). A conventional three-electrode system was employed in 0.1 M PBS at room temperature, which consisted of a platinum foil as auxiliary electrode, a saturated calomel electrode (SCE) as reference electrode, and a bare or modified GCE as working electrode. All potentials in this study are reported with respect to the SCE.

Results and discussion

3.1 Characterization of $[\text{TMPyPcCo/aCNTs}]_n$ multilayer films

The evolution of $[\text{TMPyPcCo/aCNTs}]_n$ multilayer films self-assembled on ITO glass substrate was monitored by UV-vis absorption spectra (Fig. 1). As controls, the UV-vis spectra of the $[\text{TMPyPcCo}]^{4+}$ and aCNTs dispersed in aqueous solution are also measured (the gray dashed line in Fig. 1 and Fig. S1A). Obviously, the Q-band peak at 655 nm is derived from the π - π^* transition centers on the macrocycle of $[\text{TMPyPcCo}]^{4+}$ molecule in aqueous solution. For the $[\text{TMPyPcCo/aCNTs}]_n$ multilayer films, Q-band of $[\text{TMPyPcCo}]^{4+}$ in the spectra are broadened and weakened owing to the aggregation of $[\text{TMPyPcCo}]^{4+}$ on the film. Meanwhile, an obvious red-shift of Q-band (676 nm vs. 655 nm) is observed compared with $[\text{TMPyPcCo}]^{4+}$ in aqueous solution, as a result of the electrostatic affinity between $[\text{TMPyPcCo}]^{4+}$ and aCNTs. The inset in Fig. 1 depicts the absorbance of $[\text{TMPyPcCo/aCNTs}]_n$ films at 676 nm varies linearly with respect to the bilayer number from 2 to 12 layer, indicating that the adsorbed amount of $[\text{TMPyPcCo}]^{4+}$ per bilayer is consistent.^[45] Instead, the absorbance plateau appears when the bilayer number is over 12. The results imply that the growth process for the LBL film is no longer uniform.

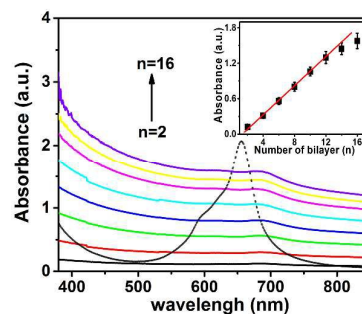


Fig. 1 UV-vis absorption spectra of the $[\text{TMPyPcCo/aCNTs}]_n$ multilayer films assembled on ITO substrates ($n = 1-16$). The gray dashed line shows the absorption of $[\text{TMPyPcCo}]^{4+}$ in aqueous solution. The absorbance of the $[\text{TMPyPcCo/aCNTs}]_n$ multilayer films at 676 nm is plotted against the bilayer number in the inset.

Raman spectroscopy can yield rich information on the quality and structure of carbon materials, especially in determining the defect and ordered-disordered structure.^[46] In order to further study the influence of $[\text{TMPyPcCo}]^{4+}$ on aCNTs, Raman spectra of the $[\text{TMPyPcCo/aCNTs}]_{12}$, $[\text{TMPyPcCo}](\text{SO}_4)_2$ and aCNTs films were recorded, respectively (Fig. 2 and Fig. S1B). Like the Raman spectrum of pure aCNTs, two strong characteristic peaks (so-called D and G bands located at $\sim 1360 \text{ cm}^{-1}$ and 1575 cm^{-1}) display in that of $[\text{TMPyPcCo/aCNTs}]_{12}$ (as shown in Fig. 2). Instead, due to the low loading in the multilayer film, only a weak and broad peak maybe ascribed to $[\text{TMPyPcCo}]^{4+}$ emerges in the range of $1000-1250 \text{ cm}^{-1}$ (Fig. S1B).^[49,50] The D-band is related to amorphous/disordered carbon (sp^3), whereas the G-band is an intrinsic feature of CNT closely originating from in-plane vibration of sp^2 carbon atoms.^[47] The intensity ratio of the D and G bands (I_D/I_G) is widely used to investigate as an indicator of the presence of defects structural in carbon materials.^[48] It is worth noting that the I_D/I_G value of $[\text{TMPyPcCo/aCNTs}]_{12}$ is very close to that of pure aCNTs (0.559 vs. 0.574). This result confirms that the functionalization of $[\text{TMPyPcCo}]^{4+}$ on the surface of aCNTs does not cause the considerable defects. In the Raman spectrum of $[\text{TMPyPcCo/aCNTs}]_{12}$ film, the G band of aCNTs up-shifted from 1571 to 1579 cm^{-1} signifies the occurrence of electron transfers from aCNTs to the adsorbed $[\text{TMPyPcCo}]^{4+}$.

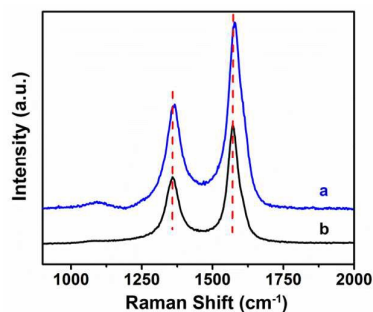


Fig. 2 The Raman spectra of $[\text{TMPyPcCo/aCNTs}]_{12}$ film on ITO substrate (a) and pure aCNTs (b).

To further gain insight into the chemical composition and their valence states of [TMPyPcCo/aCNTs]₁₂ film, XPS analyses were conducted (Fig. 3 and Fig. S2).^[51] Similar to [TMPyPcCo](SO₄)₂, C, N, O, and Co elements present in the survey spectrum of the [TMPyPcCo/aCNTs]₁₂ film, indicating the successful combination of [TMPyPcCo]⁴⁺ and aCNTs (Fig. S2A). However, the atomic ratio of N and C (N/C) in the [TMPyPcCo/aCNTs]₁₂ is 0.0633, which is considerably lower than that in pure [TMPyPcCo](SO₄)₂ film (0.114) due to the introduction of aCNTs. In addition, Co 2p_{3/2} and Co 2p_{1/2} peaks located at 781.2 and 796.0 eV can be found in the Co HRXPS, according with the typical characteristic of Co²⁺ (Fig. S2B).^[52] The high-resolution C 1s XPS (Fig. 3A) can be mainly deconvoluted into eight sub-peaks, ascribing to C-C bond of aCNTs (284.62 eV), C-OH bond (285.26 eV), C-C bond of [TMPyPcCo]⁴⁺ (285.87 eV), C-N (286.49 eV), C-O bond (287.12 eV), C=N (287.87 eV), C=O (288.64 eV) and COOH (289.53 eV), respectively.^[53] The N 1s feature of the [TMPyPcCo/aCNTs]₁₂ film are fitted with the characteristic of pyridinic-N (399.1 eV), pyrrolic-N (400.25 eV), graphitic-N (401.43 eV) and Co-coordinated-N (402.57 eV), respectively (Fig. 3B).^[54] Also, the HRXPS of O shows the obvious peak about C=O (531.45 eV) and C-O (533.27 eV) (Fig. S2C), supporting the results from C spectra.^[55]

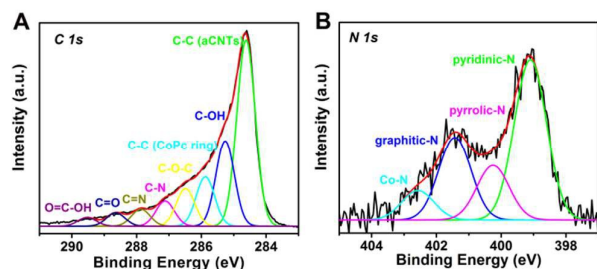


Fig. 3 The high-resolution XPS spectrum of C 1s (A) and N 1s (B) of [TMPyPcCo/aCNTs]₁₂ film.

The surface morphologies of the [TMPyPcCo/aCNTs]₁₂ film is then investigated by SEM and TEM (as shown in Fig. 4). It is clearly seen that aCNTs embedded in the [TMPyPcCo/aCNTs]₁₂ film randomly crisscross each other, and thus form 3D hierarchical network structure. Such 3D network structure not only provides an ideal rapid pathway for ion/electron transfer, but also exposes more catalytically active sites.^[56] Moreover, [TMPyPcCo]⁴⁺ can efficiently immobilize and disperse aCNTs, generating uniform layer-like structure. The thickness of the [TMPyPcCo/aCNTs]₁₂ film is about 220 nm (Fig. 4B). From the typical TEM image of the [TMPyPcCo/aCNTs]₁₂ film scaled off from the ITO substrate, the aCNTs are interlaced with one another, and the diameter of aCNTs is in the range of 12 ~ 25 nm (Fig. 4C-D). The core and walls of the aCNTs are more clearly observed in the high magnification TEM image (Fig. 4E). Besides, the surface of aCNTs is covered by discontinuous amorphous carbon, which may be attributable to the adsorption of [TMPyPcCo]⁴⁺.

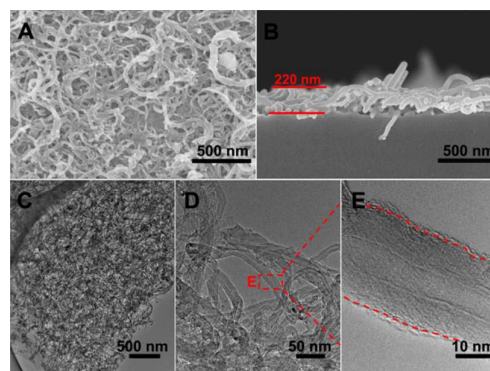


Fig. 4 (A-B) Top and cross-sectional SEM images of [TMPyPcCo/aCNTs]₁₂ film on the ITO substrate; (C-E) TEM images of [TMPyPcCo/aCNTs]₁₂ film scaled off from the ITO substrate.

3.2 Electrochemistry Characterization of the [TMPyPcCo/aCNTs]_n films

The electrochemistry character of [TMPyPcCo/aCNTs]_n multilayer films is crucial for the high-efficient sensing. To explore interface properties of [TMPyPcCo/aCNTs]_n films, the resistance change of [TMPyPcCo/aCNTs]_n films on GCEs with the LBL assembly process was firstly monitored by electrochemical impedance spectra (EIS) in 0.1 M KCl solution with 5 mM [Fe(CN)₆]^{3/4-}. As shown in Fig. 5A, only one semicircle is observed in the high-frequency region of the Nyquist plot of each multilayer film. The semicircle diameter is equal to the charge transfer resistance (R_{ct}) of [TMPyPcCo/aCNTs]_n film on the GCE, which reflects the kinetic control of the charge-transfer process at the electrode interface.^[57] Obviously, for the initial six cycles, the R_{ct} fitted by the equivalent circuit (the inset of Fig. 5A) changes from 10.31 to 72.92 Ω with the stepwise assembly of [TMPyPcCo/aCNTs]_n multilayer films; while, the R_{ct} of [TMPyPcCo/aCNTs]₁₄ is similar to that of [TMPyPcCo/aCNTs]₁₂. It, being in accord with the result of UV-Vis absorption, indicates the assembled amount is less in the seventh cycle than before. The increase of R_{ct} mainly is attribute to the restricted diffusion of the [Fe(CN)₆]^{3/4-} probe through the multilayer system related to the film permeability and the charge repulsion between electronegative aCNTs and [Fe(CN)₆]^{3/4-} probe.^[58] In view of the amount of activity sites, the [TMPyPcCo/aCNTs]₁₂ film is used as sensors to detect NO₂⁻ and H₂O₂.

The cyclic voltammograms (CVs) of the [TMPyPcCo/aCNTs]₁₂/GCE at different scan rates are shown in Fig. 5B, in order to investigate the reaction kinetics. The CVs of [TMPyPcCo/aCNTs]₁₂/GCE shows a clear well-defined reversible redox peaks corresponding to [Fe(CN)₆]^{3/4-} electron transfer process. The peak potentials of [TMPyPcCo/aCNTs]₁₂/GCE hardly changes with the scan rate, and redox peak potential difference of about 0.384 V. The ratio of I_{pa}/I_{pc} (oxidation peak current/reduction peak current) is about 1. The inset in Fig. 5B shows a linear increase of the I_{pa} and I_{pc} as the square root of the scan rate, indicating the involved electrochemical reaction is controlled by the diffusion step.^[59]

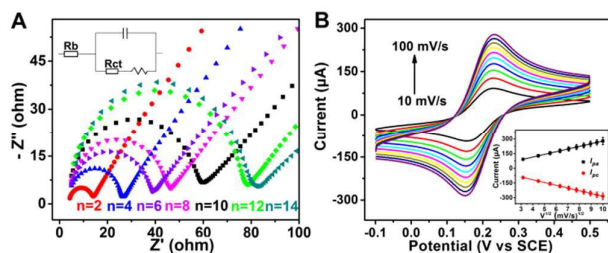
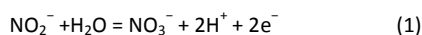


Fig. 5 (A) Nyquist plots of the [TMPyPcCo/aCNTs]_n/GCEs ($n = 2-14$) in 0.1 M KCl containing 5 mM [Fe(CN)₆]^{3/4-}; (B) CVs of the [TMPyPcCo/aCNTs]₁₂/GCE in 0.1 M KCl solution with 5 mM [Fe(CN)₆]^{3/4-} measured at different scan rates (10-100 mV·s⁻¹). Inset: the calibration plots between the anodic (black line) and cathodic (red line) peak currents vs. the scan rate ($I_{pa} = 27.1995 \times V^{1/2} + 5.3652$ (μA , mV^{1/2}·s^{-1/2}), $R^2 = 0.999$; $I_{pc} = -27.9838 \times V^{1/2} - 5.001$ (μA , mV^{1/2}·s^{-1/2}), $R^2 = 0.999$; I_{pa} , I_{pc} , and V are anodic, cathodic peak current and scan rate, respectively).

3.3 Electrochemical behaviors of NO₂⁻

The electrocatalytic sensing of the [TMPyPcCo/aCNTs]₁₂/GCE towards NO₂⁻ was studied. Fig. 6A show the typical CVs of bare GCE, [TMPyPcCo](SO₄)₂/GCE, aCNTs/GCE, and [TMPyPcCo/aCNTs]₁₂/GCE in 0.1 M PBS solution (pH = 6.2) with 1 mM NO₂⁻. The CV curve of [TMPyPcCo/aCNTs]₁₂/GCE encloses much larger area than that of bare GCE, [TMPyPcCo](SO₄)₂/GCE and aCNTs/GCE, suggesting a large specific capacitance associated with the electrochemical active surface area.^[60] These results indicate that the more active sites of [TMPyPcCo/aCNTs]₁₂/GCE are exposed and effective, a sure sign of the enhanced electrocatalytic performance obtained from [TMPyPcCo/aCNTs]₁₂ multilayer film. In contrast to the bare GCE and aCNTs/GCE, both [TMPyPcCo](SO₄)₂/GCE and [TMPyPcCo/aCNTs]₁₂/GCE generate an obvious pair of well-defined redox peaks appear at 0.08 V and -0.07 V, corresponding to the electrochemical process of Co(II)/Co(III). In addition, an irreversible oxidation peak between 0.65 V and 0.92 V is originated from the oxidation of NO₂⁻, which can be determined by measuring the CV curves with different scan rates (Fig. S3). Among all electrodes, the highest peak current and relatively smallest peak potential obtained on [TMPyPcCo/aCNTs]₁₂/GCE is mainly ascribed to the synergy role between [TMPyPcCo]⁴⁺ and aCNTs, and the 3D hierarchical network structure, which provides more active sites, a large accessible surface area, and the fast oriented transmission of charges for the sensing. Furthermore, as EIS indicated above, the bilayer-number could affect the electrocatalytic activity of [TMPyPcCo/aCNTs]_n/GCE. As shown in Fig. S4, the current responses at 0.75V are proportional to the number of bilayers ($n = 2-12$), with a linear equation: $I(\text{NO}_2^-)$ (μA) = $6.870 (\mu\text{A} \cdot \text{n}^{-1}) \times n + 47.778$ ($R^2 = 0.997$).

According to previous reports, the mechanism for NO₂⁻ oxidation on the [TMPyPcCo/aCNTs]₁₂/GCE is proposed as follows:^[28,61,62]



Apparently, the pH value has an influence on the sensing of [TMPyPcCo/aCNTs]₁₂ film. Thus, a series of CVs were recorded on the [TMPyPcCo/aCNTs]₁₂/GCE in 0.1 M PBS with 1mM NO₂⁻ at

different pH value (pH = 4.4-8.0) (Fig. S5). The current response of NO₂⁻ increases to maximum, and then decreases. PBS solution at pH 6.2 is selected as the supporting electrolyte solution. In addition, the interference of dissolved oxygen on NO₂⁻ oxidation was also studied. As shown in Fig. S6, the presence of dissolved oxygen have little effect on the NO₂⁻ oxidation.

To assess the sensitivity towards NO₂⁻, the typical amperometric responses of various electrodes were measured at 0.7 V (vs. SCE), with the successive addition of different concentrations of NO₂⁻ into the constantly stirred 0.1 M PBS (pH = 6.2). For all electrodes, the stable staircase curves display for the electrochemical response, as the NO₂⁻ concentration increases from 0.5 mM to 30 mM NO₂⁻. The current response of the [TMPyPcCo/aCNTs]₁₂/GCE, by contrast, is significantly higher than those of the bare GCE, [TMPyPcCo](SO₄)₂/GCE and aCNTs/GCE (Fig. 6B and Fig. S7). Moreover, the response current of the [TMPyPcCo/aCNTs]₁₂/GCE can be stably within 3.5 s, revealing the rapid response of the [TMPyPcCo/aCNTs]₁₂/GCE toward NO₂⁻. The calibration curve of the [TMPyPcCo/aCNTs]₁₂/GCE obtained from the I-t plot (Fig. 6C), reveals a typical well-defined behavior of a catalytic reaction with two linear range from 5 μM to 30 mM. The two linear regression equations for NO₂⁻ are expressed as: $I(\text{NO}_2^-)$ (μA) = $18.035 (\mu\text{A} \cdot \text{mM}^{-1}) \times C$ (mM) + 0.462 (0.005-10 mM, $R^2=0.998$), $I(\text{NO}_2^-)$ (μA) = $11.604 (\mu\text{A} \cdot \text{mM}^{-1}) \times C$ (mM) + 64.495 (10-30 mM, $R^2=0.998$), accompanied by the sensitivity of 18.035 and 11.604 ($\mu\text{A} \cdot \text{mM}^{-1}$), respectively. The lowest detection limit (LOD) is calculated to be 2.6 μM using the formula $\text{LOD} = 3 S/k$ (where S is the standard deviation of the blank signal, and k is the sensitivity, see experimental details in ES†). The larger linear range and lower detection limit of [TMPyPcCo/aCNTs]₁₂ layer is comparable and even superior to previously reported NO₂⁻ sensor, including Au-Pd/rGO (0.05-1000 μM , 0.02 μM), GCE/MTPAP/cit-AuNPs (0.5-4700 μM , 0.06 μM), f-ZnO@rFGO (10-8000 μM , 33 μM), etc. (see the details in Table S1, S2).

The long-term stability and reproducibility is also an important parameter for evaluating the sensing performance of [TMPyPcCo/aCNTs]₁₂/GCE. The stability of [TMPyPcCo/aCNTs]₁₂ layer was studied by the CV scanning for 100 cycles (Fig. 6D). The CV curves of the first cycle and the hundredth cycle almost overlap, indicating that the catalytic activity of [TMPyPcCo/aCNTs]₁₂/GCE is very stable. Meanwhile, the [TMPyPcCo/aCNTs]₁₂/GCE is also stored in air at room temperature for 40 days, and its current response to 1 mM NO₂⁻ is assessed every five days. Only a small loss (about 3.65%) of current response is produced after the long-term storage (the inset of Fig. 6D), suggesting the high actual operability for NO₂⁻ determining.

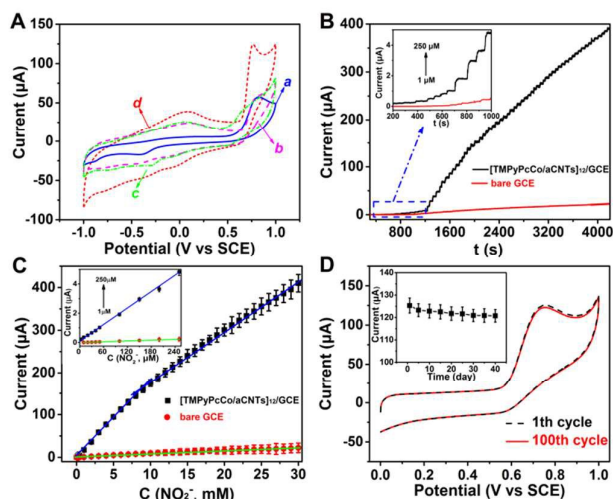


Fig. 6 (A) CVs of GCE (a), [TMPyPcCo](SO₄)₂/GCE (b), aCNTs/GCE (c) and [TMPyPcCo/aCNTs]₁₂/GCE (d) in 0.1 M PBS (pH = 6.2) solution containing 1 mM NO₂⁻, scan rate: 50 mV·s⁻¹. (B) Amperometric response of the [TMPyPcCo/aCNTs]₁₂/GCE and bare GCE (holding at 0.7 V vs. SCE) for the successive additions of 0.5 mM to 30 mM NO₂⁻ into continuously stirred 0.1 M PBS (pH = 6.2). (C) The corresponding linear calibration relationship of the current response vs. the concentration of NO₂⁻. (D) CVs of the [TMPyPcCo/aCNTs]₁₂/GCE in 0.1 M PBS (pH = 6.2) solution with 1 mM NO₂⁻ obtained at the first cycle and the hundredth cycle, respectively; the inset is the stability experiment of the [TMPyPcCo/aCNTs]₁₂/GCE to detect 1 mM NO₂⁻ for 40 days (holding at 0.7 V vs. SCE).

As another important indicator of practical application, the selectivity for NO₂⁻ detection was also investigated by amperometric measurements. As shown in Fig. 7, the current response of the [TMPyPcCo/aCNTs]₁₂/GCE significantly increases after adding 0.5 mM NO₂⁻ into the PBS solution (pH = 6.2), while the current response to the successive addition of various interferents, such as K₂CO₃, NaSO₃, CaCl₂, MgSO₄, AgCl, BaCl₂, NH₄Cl, CH₃COONa, KIO₃, urea, glucose, citric acid, and glutamic acid, at a 100-fold concentration (50 mM) is negligible. Instead, a significant current response can be observed after the subsequent addition of 0.5 mM of NO₂⁻, which is similar to the initial response. The result implies that the interferents have no impact on the NO₂⁻ detection performance. Four real samples of tap water are performed by standard addition method to evaluate the analytical applicability of the proposed method. The samples were mixed with 0.1 M PBS (pH = 6.2) for NO₂⁻ determination, and the results are listed in Table S3. The recovery of four samples is between 100.9 and 106.2%, which proved that the electrode can be practically applied in NO₂⁻ determining of real samples.

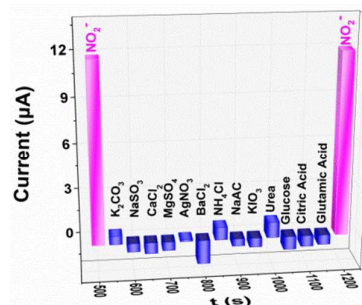
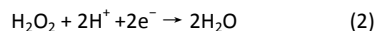


Fig. 7 The current response of [TMPyPcCo/aCNTs]₁₂/GCE to the addition of various interferents to 50 mL of 0.10 M PBS solution (pH = 6.2) at 0.7 V.

3.4 Electrochemical behaviors of H₂O₂

Besides NO₂⁻ sensing, the [TMPyPcCo/aCNTs]₁₂/GCE can also be used to detect H₂O₂. Fig. 8A shows the CVs of [TMPyPcCo/aCNTs]₁₂/GCE, aCNTs/GCE, [TMPyPcCo](SO₄)₂/GCE, and bare GCE in 0.1 M PBS solution (pH=7.0) containing 1 mM H₂O₂ (scan rate: 50 mV·s⁻¹). Compared with other electrodes, [TMPyPcCo/aCNTs]₁₂/GCE generates an obvious reduction peak at around -0.25 V. The current responses at -0.25V are also proportional to the number of bilayers (n = 2-12), with a linear equation: $I(\text{H}_2\text{O}_2, \mu\text{A}) = -0.183 (\mu\text{A}\cdot\text{n}^{-1}) \times n + 10.639$ ($R^2 = 0.996$) (Fig. S8). Furthermore, the irreversible reduction reaction of H₂O₂ on [TMPyPcCo/aCNTs]₁₂/GCE is controlled by diffusion, and untouched by the dissolved oxygen, as evidenced by the CVs in Fig. S9 and S10. The mechanism for the H₂O₂ reduction on the [TMPyPcCo/aCNTs]₁₂/GCE is proposed as follows:^[63,64]



A series of differential pulse voltammograms (DPVs) were also recorded on the aCNTs/GCE, [TMPyPcCo](SO₄)₂/GCE and [TMPyPcCo/aCNTs]₁₂/GCE at various concentrations of H₂O₂. As shown in Fig. 8B and Fig. S11, with increasing H₂O₂ concentration, the current response on pure [TMPyPcCo](SO₄)₂/GCE and [TMPyPcCo/aCNTs]₁₂/GCE at about -0.25V significant increases, whereas the current response on pure aCNTs/GCE decreases. To evaluate the catalytic activity towards H₂O₂ in detail, the calibration curve of [TMPyPcCo/aCNTs]₁₂/GCE obtained from DPVs are shown in the inset of Fig. 8B. A distinct current plateau can be observed when the H₂O₂ concentration is higher than 0.8 mM. The linear regression equations for H₂O₂ is expressed as $I(\text{H}_2\text{O}_2, \mu\text{A}) = -1.61028 (\mu\text{A}\cdot\text{mM}^{-1}) \times C (\text{mM}) - 10.7838$ ($R^2 = 0.9958$). The detection limit and sensitivity is 2.8 μM (S/N = 3) and 1.61028 μA·mM⁻¹, respectively, which are derived from the calibration curve. The linear range and detection limit of the [TMPyPcCo/aCNTs]₁₂/GCE, superior to other sensors, are comparable to the most previously reported H₂O₂ sensors (Table S4, S5).

Furthermore, as H₂O₂ sensor, the [TMPyPcCo/aCNTs]₁₂/GCE also deliver superior cycling stability and reproducibility as revealed by nearly the same CV scanning current for 100 cycles and a smaller current loss of 4.08 % after stored in air at room temperature for 40 days (Fig. 8C). Meanwhile, compared with 0.5 M H₂O₂, the interferences with 50 M cannot give rise to the remarkable current,

suggesting the good selectivity for H_2O_2 detection (as shown in Fig. 8D). The excellent sensitivity and selectivity for H_2O_2 signify that [TMPyPcCo/aCNTs]₁₂/GCE could be applied to determine H_2O_2 in real samples. For the four real samples of tap water prepared by standard addition method, the recovery is between 95.3 and 109.0 % (Table S6). Therefore, it is promising as a biosensor to achieve quantitative detection of H_2O_2 in practical applications.

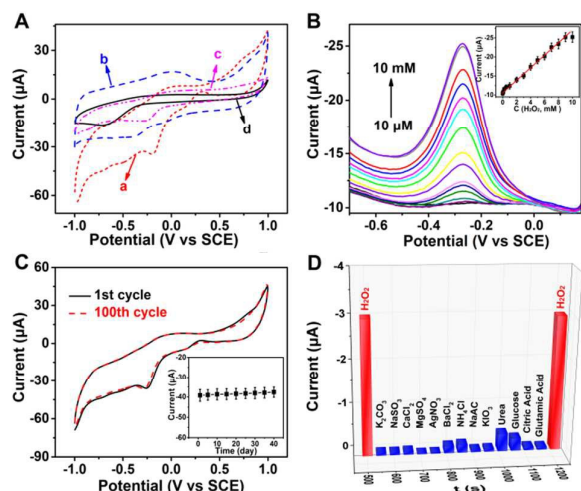


Fig. 8 (A) CVs of [TMPyPcCo/aCNTs]₁₂/GCE (a), aCNTs/GCE (b), [TMPyPcCo](SO₄)₂/GCE (c), and bare GCE (d) in 0.1 M PBS (pH = 7.0) solution containing 1 mM H_2O_2 , scan rate: 50 mV·s⁻¹. (B) DPVs response for different concentration of H_2O_2 at the [TMPyPcCo/aCNTs]₁₂/GCE in 0.1M PBS solution (pH = 7.0); the inset shows the calibration linear relationship of the current response vs. the H_2O_2 concentration. (C) CVs of the [TMPyPcCo/aCNTs]₁₂/GCE in 0.1 M PBS (pH = 7.0) solution with 1 mM H_2O_2 obtained at the first cycle and the hundredth cycle, respectively; the inset is the stability experiment of the [TMPyPcCo/aCNTs]₁₂/GCE to detect 1 mM H_2O_2 for 40 days (holding at -0.25 V vs. SCE). (D) The current response of [TMPyPcCo/aCNTs]₁₂/GCE to the addition of various interferents to 50 mL of 0.10 M PBS solution (pH = 7.0) at -0.25 V.

Conclusions

We have demonstrated the fabrication and application of [TMPyPcCo/aCNTs]₁₂/GCE for NO_2^- and H_2O_2 electrochemical biosensors. The formation of layer-by-layer [TMPyPcCo/aCNTs]₁₂/GCE is ascribes to the direct electrostatic interaction assembly between [TMPyPcCo]⁴⁺ and aCNTs without any polymer binders. The [TMPyPcCo/aCNTs]₁₂/GCE displays excellent electrocatalytic activity, stability, reproducibility and selectivity for NO_2^- oxidation and H_2O_2 reduction. The enhanced effectiveness attributes to the loose interlaced, and accurate structure, and the synergistic effect of [TMPyPcCo]⁴⁺ and aCNTs, which could offer the large accessible surface area, more exposed active sites and the oriented transmission of electrons, as well as the unimpeded

pathways for matter diffusion. In addition, the highly active [TMPyPcCo/aCNTs]₁₂/GCE can be used for quantitative detection of NO_2^- and H_2O_2 in practical applications, suggesting a promising candidate for the NO_2^- and H_2O_2 biosensor.

Acknowledgements

This work was financially supported by the National Natural Science Foundation of China (51002046, 51102082, 51202061 and 21573062), the Natural Science Foundation for the Natural Science of Heilongjiang Province of China (LC2012C02 and B201308), the Research Fund of Heilongjiang Provincial Education Department (12511377 and 12521399), the Postdoctoral Science-Research Developmental Foundation of Heilongjiang Province (LBH-Q11015) and the Innovative Talents Program for the Returned Overseas Scholars of Harbin of China (2012RFLXG031).

References

- X. C. Dong, H. Xu, X. W. Wang, Y. X. Huang, M. B. Chan-Park, H. Zhang, L. H. Wang, W. Huang, P. Chen, *ACS Nano*, 2012, **6**, 3206-3213.
- C. Z. Zhu, S. J. Guo, S. J. Dong, *Adv. Mater.*, 2012, **24**, 2326-2331.
- D. Seth, A. Hausladen, Y. J. Wang, J. S. Stamler, *Science*, 2012, **336**, 470-473.
- A.S. Serraa, S.R. Jorgea, C.M. Silveiraa, J.J.G. Mouraa, E. Jubeteb, E. Ochotecob, G. Cabañero, H. Grandeb, M.G. Almeidaa, *Analytica Chimica Acta*, 2011, **693**, 41-46.
- L. S. Engel, w. h. Chow, T. L. Vaughan, M. D. Gammon, H. A. Risch, J. L. Stanford, J. B. Schoenberg, S. T. Mayne, R. Dubrow, H. Rotterdam, A. B. West, M. Blaser, W. J. Blot, M. H. Gail, J. F. Fraumeni, *J. Natl. Cancer I.*, 2003, **95**(18), 1404-1413.
- A. J. Cross, L. M. Ferrucci, A. Risch, B. I. Graubard, M. H. Ward, Y. Park, A. R. Hollenbeck, A. Schatzkin, R. Sinha, *Cancer Res.*, 2010, **70**, 2406-2414.
- M. M. Liu, R. Liu, W. Chen, *Biosens. Bioelectron.*, 2013, **45**, 206-212.
- Y. X. Liu, X. C. Dong, P. Chen, *Chem. Soc. Rev.*, 2012, **41**, 2283-2307.
- Z. Lin, W. Xue, H. Chen, J. M. Lin, *Anal. Chem.*, 2011, **83**, 8245-8251.
- L. J. Gimbert, P. J. Worsfold, *TRAC-Trend. Anal. Chem.*, 2007, **26**, 914-930.
- M. C. Breadmore, C. Michael, A. I. Shallan, H. R. Rabanes, D. Gstoettenmayr, A. S. A. Keyon, A. Gaspar, M. Dawod, J. P. Quirino, *Electrophoresis*, 2013, **34**, 29-54.
- E. Isarain-Chavez, C. Arias, P. L. Cabot, F. Centellas, R. M. Rodriguez, J. A. Garrido, E. Brillas, *Appl. Catal. B : Environ.*, 2010, **96**, 361-369.
- D. Y. Zhai, B. R. Liu, Y. Shi, L. J. Pan, Y. Q. Wang, W. B. Li, R. Zhang, G. H. Yu, *ACS NANO*, 2013, **7**, 3540-3546.
- D. Chen, H. B. Feng, J. H. Li, *Chem. Rev.*, 2012, **112**, 6027-6053.
- S. Radhakrishnan, K. Krishnamoorthy, C. Sekar, J. Wilson, S. J. Kim, *Appl. Catal. B : Environ.*, 2014, **148-149**, 22-28.
- S. Radhakrishnan, C. Sumathi, A. Umar, S. J. Kim, J. Wilson, V. Dharuman, *Biosens. Bioelectron.*, 2013, **47**, 133-140.
- X. Q. Liu, H. Q. Feng, R. X. Zhao, Y. B. Wang, X. H. Liu, *Biosens. Bioelectron.*, 2012, **31**, 101-104.
- V. Gribova, R. Auzely-Velty, C. Picart, *Chem. Mater.*, 2012, **24**, 854-869
- L. X. Guo, Z. M. Chen, J. L. Zhang, H. Wu, F. Wu, C. Y. He, B. Wang, Y. Q. Wu, *RSC Adv.*, 2015, **5**, 23283-23290.

- 20 W. J. Lian, S. Liu, J. H. Yu, X. R. Xing, J. Li, M. Cui, J. D. Huang, *Biosens. Bioelectron.*, 2012, **38**, 163-169.
- 21 W. Chidawanyika, T. Nyokong, *Carbon*, 2010, **48**, 2831-2838.
- 22 I. Obraztsov, K. Noworyta, A. Hart, H. B. Gobeze, C. B. Kc, W. Kutner, F. D'Souza, *ACS Appl. Mater. Interfaces*, 2014, **6**, 8688-8701.
- 23 C. Zhang, Y. H. Hong, R. H. Dai, X. P. Lin, L. S. Long, C. Wang, W. B. Lin, *ACS Appl. Mater. Interfaces*, 2015, **7**, 11648-11653.
- 24 X. Huang, Z. Y. Zeng, Z. X. Fan, J. Q. Liu, H. Zhang, *Adv. Mater.*, 2012, **24**, 5979-6004.
- 25 K. Ariga, Q. M. Ji, M. J. McShane, Y. M. Lvov, A. Vinu, J. P. Hill, *Chem. Mater.*, 2012, **24**, 728-737.
- 26 G. Bottari, G. de la Torre, D. M. Guldi, T. Torres, *Chem. Rev.*, 2010, **110**, 6768-6816.
- 27 Y. Chen, M. Hanack, Y. Araki, O. Ito, *Chem. Soc. Rev.*, 2005, **34**, 517-529.
- 28 P. Li, Y. Ding, A. Wang, L. Zhou, S.H. Wei, Y. M. Zhou, Y. W. Tang, Y. Chen, C. X. Cai, T. H. Lu, *ACS Appl. Mater. Interfaces*, 2013, **5**, 2255-2260.
- 29 J. H. Zagal, S. Griveau, J. F. Silva, T. Nyokong, F. Bedioui, *Coord. Chem. Rev.*, 2010, **254**, 2755-2791.
- 30 W. Y. Lu, N. Li, W. X. Chen, Y. Y. Yao, *Carbon*, 2009, **47**, 3337-3345.
- 31 U. N. Maiti, W. J. Lee, J. M. Lee, Y. Oh, J. Y. Kim, J. E. Kim, J. Shim, T. H. Han, S. O. Kim, *Adv. Mater.*, 2014, **26**, 40-67.
- 32 T. Morimoto, S. K. Joung, T. Saito, D. N. Futaba, K. Hata, T. Okazaki, *ACS Nano*, 2014, **8**, 9897-9904.
- 33 M. A. Kabbani, C. S. Tiwary, P. A. S. Autreto, G. Brunetto, A. Som, K. R. Krishnadas, S. Ozden, K. P. Hackenberg, Y. I. Gong, D. S. Galvao, *Nat. Common.*, 2015, **6**, 7291.
- 34 Q. Liu, J. Q. Tian, W. Cui, P. Jiang, N. Y. Cheng, A. M. Asiri, X. P. Sun, *Angew. Chem. Int. Ed.*, 2014, **53**, 6710-6714.
- 35 S. Nardecchia, D. Carriazo, M. L. Ferrer, M. C. Gutierrez, F. del Monte, *Chem. Soc. Rev.*, 2013, **42**, 794-830.
- 36 M. Shi, Z. M. Chen, L. X. Guo, X. H. Liang, J. L. Zhang, C. Y. He, B. Wang and Y. Q. Wu, *J. Mater. Chem. B*, 2014, **2**, 4876-4882.
- 37 P. Jiang, Q. Liu, Y. H. Liang, J. Q. Tian, A. M. Asiri, X. P. Sun, *Angew. Chem. Int. Ed.*, 2014, **53**, 12855-12859.
- 38 J. Q. Tian, Q. Liu, N. Y. Cheng, A. M. Asiri, X. P. Sun, *Angew. Chem. Int. Ed.*, 2014, **53**, 9577-9581.
- 39 W. J. Tong, X. X. Song, C. Y. Gao, *Chem. Soc. Rev.*, 2012, **41**, 6103-6124.
- 40 S. Y. Kim, J. Hong, R. Kaviani, S. W. Lee, M. N. Hyder, Y. Shao-Horn, P. T. Hammond, *Energy Environ. Sci.*, 2013, **6**, 888-897.
- 41 G. K. Such, A. P. R. Johnston, F. Caruso, *Chem. Soc. Rev.*, 2011, **40**, 19-29.
- 42 B. Yuan, H. Yang, Z. Q. Wang, X. Zhang, *Langmuir*, 2014, **30**, 15462-15467.
- 43 H. H. Wang, Y. Bu, W. L. Dai, K. Li, H. D. Wang, X. Zuo, *Sensors and Actuators B*, 2015, **216**, 298-306.
- 44 D. K. Huang, J. F. Lu, S. H. Li, Y. P. Luo, C. Zhao, B. Hu, M. K. Wang, Y. Shen, *Langmuir*, 2014, **30**, 6990-6998.
- 45 G. Lee, D. Kim, J. Yun, Y. Ko, J. Cho, J. S. Ha, *Nanoscale*, 2014, **6**, 9655-9664.
- 46 L. M. He, P. P. Zhao, Q. Han, X. Y. Wang, X. Cai, Y. F. Shi, L. B. Zhou, Y. M. Zhang, W. Xue, *Carbon*, 2013, **56**, 224-234.
- 47 N. He, Y. Chen, J. R. Bai, J. Wang, W. J. Blau, J. H. Zhu, *J. Phys. Chem. C*, 2009, **113**, 13029-13035.
- 48 B. P. Vinayan, R. Nagar, V. Raman, N. Rajalakshmi, K. S. Dhathathreyanb, S. Ramaprabhu, *J. Mater. Chem.*, 2012, **22**, 9949-9956.
- 49 M. Szybowski, W. Bała, S. Dümecke, K. Fabisiak, K. Paprocki, M. Drozdowski, *Thin Solid Films*, 2011, **520**, 623-627.
- 50 M. Szybowski, T. Runka, M. Drozdowski, W. Bała, A. Grodzicki, P. Piszczek, A. Bratkowski, *J. Mol. Struct.*, 2004, **704**, 107-113.
- 51 B. Devadas, R. Madhu, S. M. Chen, H. T. Yeh, *J. Mater. Chem. B*, 2014, **2**, 7515-7523.
- 52 L. Q. Jiang, M. Li, L. Lin, Y. F. Li, X. Q. He, L. L. Cui, *RSC Adv.*, 2014, **4**, 26653-26661.
- 53 M. E. Lipinska, S. L. H. Rebelo, C. Freire, *J. Mater. Sci.*, 2014, **49**, 1494-1505.
- 54 P. Kumar, A. Kumar, B. Sreedhar, ; B. Sain, S. S. Ray, S. L. Jain, *Chem. Eur. J.*, 2014, **20**, 6154-616 P. Kumar, A. Kumar, B. Sreedhar, ; B. Sain, S. S. Ray, S. L. Jain, *Chem. Eur. J.*, 2014, **20**, 6154-616.
- 55 H. A. Miller, M. Bevilacqua, J. Filippi, A. Lavacchi, A. Marchionni, M. Marelli, S. Moneti, W. Oberhauser, E. Vesselli, M. Innocenti, *J. Mater. Chem. A*, 2013, **1**, 13337-13347.
- 56 M. N. Hyder, R. Kaviani, Z. Sultana, K. Saetia, P. Y. Chen, S. W. Lee, Y. Shao-Horn, P. T. Hammond, *Chem. Mater.*, 2014, **26**, 5310-5318.
- 57 J. B. Han, X. Y. Xu, X. Y. Rao, M. Wei, D. G. Evans, X. Duan, *J. Mater. Chem.*, 2011, **21**, 2126-2130.
- 58 Z. Chang, M. Chen, H. Fan, K. Zhao, S. Q. Zhuang, P. G. He, Y. Z. Fang, *Electrochimica Acta*, 2008, **53**, 2939-2945.
- 59 K. Y. Hwa, B. Subramani, *Biosens. Bioelectron.*, 2014, **62**, 127-133.
- 60 M. Grden, M. Alsabet, G. Jerkiewicz, *ACS Appl. Mater. Interfaces*, 2012, **4**, 3012-3021.
- 61 X. R. Li, F. Y. Kong, J. Liu, T. M. Liang, J. J. Xu, H. Y. Chen, *Adv. Funct. Mater.*, 2012, **22**, 1981-1988.
- 62 H. Liu, C. Y. Duan, X. Su, X. N. Dong, Z. Huang, W. Q. Shen, Z. F. Zhu, *Sens Actuators B Chem.*, 2014, **203**, 303-310.
- 63 W. R. P. Barros, R. M. Reis, R. S. Rocha, M. R. V. Lanza, *Electrochimica Acta*, 2013, **104**, 12-18.
- 64 S. N. Azizi, S. Ghasemi, A. Samadi-Maybodi, M. Ranjbar-Azad, *Sens Actuators B Chem.*, 2015, **216**, 271-278.

Graphical Abstract

